

Impact of Humidity on Water Dynamics and Electrical Conductivity in PEDOT:PSS/Cellulose Nanofibril Nanocomposite Films: Insights from Quasi-Elastic Neutron Scattering

Lucas P. Kreuzer,* Marie Betker, Marcell Wolf, Bart-Jan Niebuur, Jacques Ollivier, L. Daniel Söderberg, and Stephan V. Roth



Cite This: *Macromolecules* 2025, 58, 2247–2258



Read Online

ACCESS |



Metrics & More

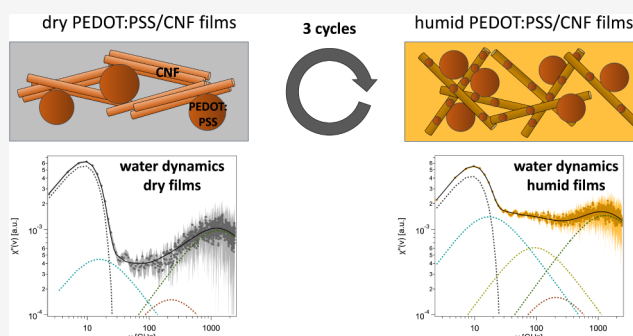


Article Recommendations



Supporting Information

ABSTRACT: The water dynamics in a nanocomposite film that consists of the electrically conductive poly(3,4-ethylene dioxythiophene):poly(styrenesulfonate) (PEDOT:PSS) and cellulose nanofibrils (CNFs) have been investigated during three cycles of exposure to low and high relative humidity (RH = 5% and 85%, respectively) using quasi-elastic neutron scattering (QENS). The obtained dynamical structure factors are transformed into the imaginary part of the dynamic susceptibility to better differentiate between the individual relaxation processes. In a humid environment, two different water species are present inside the films: fast-moving bulk water and slow-moving hydration water. During the first cycle, a large amount of hydration water enhances the polymer chain mobility, eventually leading to irreversible structural rearrangements within the film. In the subsequent cycles, we observed a release of all bulk water and portions of hydration water upon drying, along with an uptake of both water species in a humid environment. The relaxation times of hydration water diffusion as a function of momentum transfer can be described by a jump-diffusion model. The obtained jump lengths, residence times, and diffusion coefficients of hydration water suggest a change in the hydration layer upon drying: water molecules around hydrophobic groups are released from the film, while the hydrogen bonds between water and hydrophilic groups are sufficiently strong to keep these molecules inside the films, even in a dry state. The QENS results can be correlated to the structural and conductive properties. In the dry state, the low hydration water content and the absence of bulk water allow for improved wetting of the CNFs by PEDOT:PSS, which eventually increases the electrical conductivity of the films.



INTRODUCTION

Poly(3,4-ethylenedioxythiophene):poly(styrenesulfonate) (PEDOT:PSS) is a water-soluble and electrically conductive polymer that is increasingly applied in organic electronics across numerous fields, such as batteries, supercapacitors, and solar cells.^{1–3} Many studies focus on the optimization of device performance regarding conductivity, charging and recharging times, and initial mechanical stability and flexibility. Long-term degradation issues as a result of, e.g., humid environments, however, are rarely discussed. In recent studies, it has been shown that pure PEDOT:PSS films absorb significant amounts of water (over 50 vol %), which is accompanied by pronounced swelling (increase in film thickness by a factor of up to 1.6).^{4,5} Consequently, the PEDOT:PSS films experience strong internal stresses, resulting in structural degradation and a loss of device performance. One approach to overcome this is the integration of soft PEDOT:PSS into a matrix of organic nanofibers. Besides well-described matrices, such as nanofibers or nanotubes composed of silver, carbon, or PEDOT:PSS itself,^{6–9} cellulose nanofibrils (CNFs) gain more

and more attention as they combine advantageous properties such as mechanical stiffness, lightweight performance, and flexibility.^{10,11} As described by Isogai et al., CNFs can be prepared by the (2,2,6,6-tetramethylpiperidinyl-1-oxyl) (TEMPO) mediated oxidation procedure, which results in CNFs with controllable surface charges.¹² By chemical modification, the surface charge—and thus, the surface properties, such as contact angle and surface free energy—can be tuned.^{13,14} Overall, CNF as a host matrix for electrically conductive polymers has been studied in great detail and used in electrochemical circuits, mixed ionic-electronic conductors,

Received: October 1, 2024
Revised: January 17, 2025
Accepted: February 3, 2025
Published: February 18, 2025



conductive aerogels as electrodes, and paper-based conductive microfluidics.^{15–18}

Integrating PEDOT:PSS into a CNF film strongly hindered film swelling, although a certain amount of water was still absorbed.¹⁹ Exposing the films to three cycles of high and low humidity (95% and 5%, respectively) resulted in water uptake and irreversible changes in the nanostructure during the first cycle, while during the remaining two cycles, switching between high and low humidity led to reversible structural rearrangements.¹⁹ Moreover, a direct correlation between the film's nanostructure and the macroscopic electrical conductivity was established, which offers the possibility to optimize their performance during device use by gaining control over the nanostructure.

For the nanostructure and macroscopic functionality of cellulose-based materials in general, the interaction with water, especially with hydration water, is of fundamental importance as it greatly influences the chain mobility and determines the ratio of exposed hydrophilic and hydrophobic surfaces.^{20–27} The chemical structures of PEDOT:PSS and cellulose are shown in Figure 1. To fully understand and eventually control

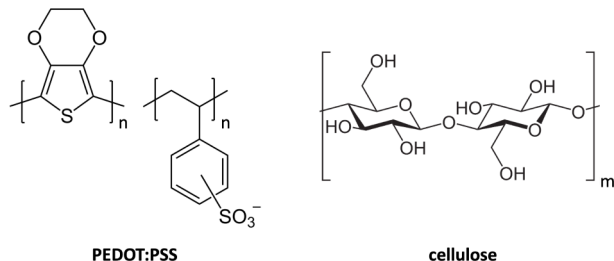


Figure 1. Chemical structure of PEDOT:PSS (left) and cellulose (right), from which the PEDOT:PSS/CNF nanocomposite films are prepared, is shown. PEDOT:PSS bears a hydrophilic sulfonate ($-\text{SO}_3^-$) group, while cellulose exhibits several primary ($-\text{CH}_2\text{OH}$) and secondary hydroxyl groups ($-\text{OH}$). These groups are hydrogen bonds with water, while the other groups feature hydrophobic interactions with water upon hydration. CNFs are prepared according to ref 12.

the structural rearrangements observed in PEDOT:PSS/CNF films upon changing relative humidity, a detailed study of hydration water is crucial. In previous studies, the diffusion of hydration water molecules was shown to proceed through jumps between cages made from neighboring water molecules. In between these jumps, the water molecules are stationary and perform local motions.^{28–32} However, due to the presence of macromolecular structures, the motion of hydration water molecules is spatially and/or temporally hindered.^{28,31} Surface charges and the respective counterions (both present in CNFs due to the TEMPO-mediated oxidation) may further increase the complexity of the interactions between hydration water and macromolecules.³³ Besides the nature of the macromolecule, surface charges, and counterion type and concentration, the sample geometry also plays a role: confinement and interface effects are much more pronounced in consolidated film systems as compared to aqueous solutions, which lead to significantly different properties of the same polymer, such as a shift in phase transition temperatures or an altered affinity to certain solvents.^{34,35} Thus, it is impossible to assume or extrapolate a certain behavior of the same polymer from, e.g., an aqueous solution to a film geometry.

Besides hydration water, we expect bulk water within the PEDOT:PSS/CNF films as well. Here, we define hydration water as water molecules in close vicinity to PEDOT:PSS/CNF, and bulk water as water molecules that interact with only other water molecules. The diffusion behavior of hydration water and bulk water is markedly different. Therefore, quasi-elastic neutron scattering (QENS) is employed here to study both, as it covers relevant time and length scales. To resolve the water dynamics, an energy window was selected that spans more than 3 orders of magnitude in frequency. The obtained dynamic structure factors were transformed into the imaginary part of the dynamic susceptibilities, allowing a straightforward separation of the dynamics of hydration and bulk water as a function of the relative humidity.³⁶

With this study, we investigate the water dynamics within electrically conductive PEDOT:PSS/CNF films in changing relative humidity. From the obtained water dynamics, we can deduce the water–PEDOT:PSS/CNF interactions. In particular, hydration water is shown to play a crucial role, e.g., in the flexibility, mobility, and eventually the structure and functionality of the polymer chains. This becomes even more important for polymer films, where the amount of hydration water and, thus, the polymer mobility, is limited. In addition, the hydration of polymers is generally not well understood, and even less so in a film geometry, where confinement and interface effects lead to altered water–polymer interactions. By correlating the obtained results with existing information about the film morphology and electrical conductivity,¹⁹ we aim to further resolve the nature of water–PEDOT:PSS/CNF interactions, to understand the structure–dynamics relationship in PEDOT:PSS/CNF nanocomposite films, and how it influences macroscopic material properties, such as electrical conductivity. Thereby, we contribute to the design of novel organic electronics and the optimization of existing ones. Moreover, the derived physical parameters regarding the jump-like water movement within the PEDOT:PSS/CNF film are valuable as input for future research on PEDOT:PSS/CNF films, for example, using molecular dynamics simulations.

RESULTS AND DISCUSSION

PEDOT:PSS/CNF films were prepared via spray-coating deposition onto a heated (110 °C) Si substrate. After being dried, the films were removed from the substrate by means of sharp tweezers. Details of the preparation routine can be found in the [Experimental Section](#) and ref 37. The free-standing PEDOT:PSS/CNF films were characterized via optical microscopy (OM), atomic force microscopy (AFM), and scanning electron microscopy (SEM). The respective microscopy images can be found in Figures S1–S3. All employed microscopy techniques confirm a homogeneously mixed PEDOT:PSS/CNF surface topography, which agrees with previous work.¹⁹ These results also show a homogeneously mixed bulk morphology, which we assume for the present work. The mean square surface roughness obtained via AFM is low (2.9 ± 0.6 nm) with respect to the film thickness of approximately 10 μm .

Here, we investigate the water dynamics in PEDOT:PSS/CNF films at 25 °C using QENS, during three cycles of almost dry (relative humidity (RH) = 5%) and humid (RH = 85%) H₂O environments. This set of QENS measurements is labeled Experiment A. Figure 2 shows the general measurement protocol. QENS is sensitive to the diffusive motions of atoms, particularly hydrogen, due to a large incoherent neutron

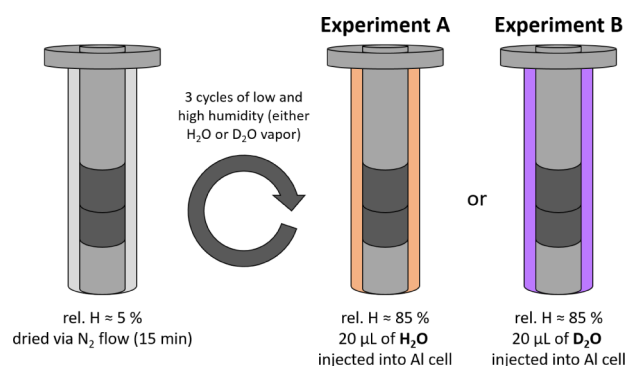


Figure 2. Overview of the experimental protocol. Two individual experiments have been performed, in which the PEDOT:PSS/CNF films were exposed to overall three cycles of low and high humidity ($\text{RH} \approx 5$ and 85%). To humidify the surrounding of the PEDOT:PSS/CNF films, $20 \mu\text{L}$ of H_2O (Experiment A) or D_2O (Experiment B) was added into the measurement cells. In this way, it is assured that in Experiment A mainly water diffusion is measured, as is explained in the main text. Further information about the mounting of the PEDOT:PSS/CNF films in the standard hollow cylinder cells can be found in the [Experimental Section](#).

scattering cross-section. One has to note that other dynamics of hydrogen atoms that belong to the PEDOT:PSS/CNF nanocomposite might contribute to the obtained QENS signal as well, even though the literature reports that they occur on time scales that are much longer than the diffusion of water.^{38,39} To be able to distinguish these from H_2O dynamics, we performed a second experiment, where the PEDOT:PSS/CNF films have been exposed to three cycles of high humidity using D_2O ($\text{RH} = 85\%$) and an almost dry ($\text{RH} = 5\%$) environment (Experiment B). Deuterium has a significantly smaller incoherent neutron scattering cross-section than hydrogen, and thus, Experiment B reveals which part of the measured signal stems from PEDOT:PSS/CNF dynamics.

In Experiment B, the PEDOT:PSS/CNF film features a similar scattering pattern compared to the film in a humid H_2O environment, but with a lower intensity (see [Figure S6](#)). Despite the low scattering intensity, no further relaxation processes are detected, which indicates that our QENS experiments in a humid H_2O environment (Experiment A) mainly detect water dynamics. As was already mentioned earlier, this assumption is supported by literature, as corresponding polymer dynamics are typically found at low energy transfers ($0.2\text{--}1.8 \text{ GHz}$), which are beyond the INS resolution limit.^{38,39} For a more detailed analysis of Experiment B, please see the [Supplementary Information](#). In addition, the QENS spectrum of an empty cell under high humid conditions at $25 \text{ }^\circ\text{C}$ is used as a reference to better distinguish between water inside and outside the film.

Figure 3 shows the dynamic structure factors $S(q, \Delta E)$ as a function of energy transfer at $q = 1.5 \text{ \AA}^{-1}$ of pure H_2O vapor (blue curve), and of the PEDOT:PSS/CNF films during the first cycle of exposure to low (gray) and high H_2O humidity (orange). Clear differences are observed between all three curves, which are discussed in the following.

At very low energy transfers (between -0.15 and -0.10 meV), the dynamic structure factor of the PEDOT:PSS/CNF films in both humid and dry environments features a higher intensity compared to pure H_2O vapor. This difference is especially pronounced for the film exposed to high H_2O humidity and indicates the presence of a slowly moving water species.

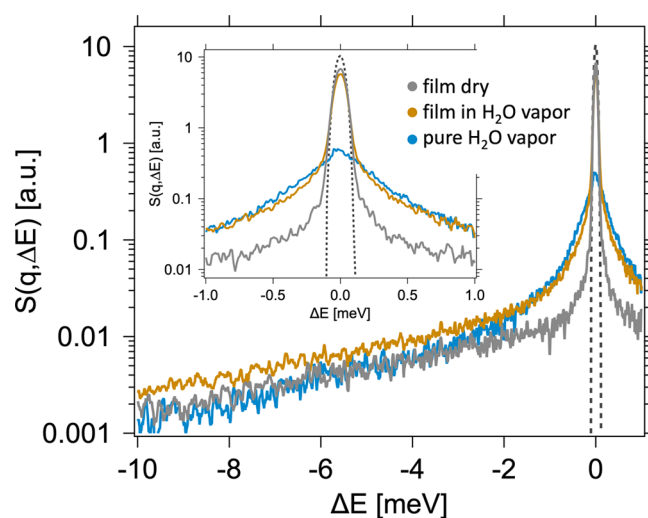


Figure 3. Dynamic structure factor $S(q, \Delta E)$ of H_2O (blue line) and PEDOT:PSS/CNF exposed to low (gray line) and high (orange full line) humidity at $q = 1.5 \text{ \AA}^{-1}$. The temperature was set to $25 \text{ }^\circ\text{C}$. The black-dashed line represents the elastic line, which was determined during a reference measurement on vanadium. The background of the vanadium measurement is lower than 0.001.

Furthermore, we observe an increased scattering intensity of the pure H_2O vapor between intermediate energy transfers of -1.1 and -0.15 meV , whereas at higher energy transfers, the scattering intensity of the films equals or exceeds the intensity of pure H_2O vapor. This indicates that the dynamical structure factor shown represents multiple relaxation processes. To better distinguish between them, the dynamic structure factor is transformed into the imaginary part of the corresponding susceptibility $\chi''(q, \nu)$, which is a common evaluation method for QENS data of biomacromolecules and polymers in aqueous solution.^{40–44} Detailed descriptions of the transformation can be found in the literature.^{36,40–42} The respective susceptibilities are shown in [Figure 4](#). In the following, all data are analyzed and discussed in terms of $\chi''(q, \nu)$. First, the data on pure H_2O vapor will be discussed, before we move on to a detailed analysis of the water dynamics within the PEDOT:PSS/CNF films. Eventually, we put our findings in context with structural features of the PEDOT:PSS/CNF films and their electrical conductivity.

Dynamics of Pure H_2O Vapor. QENS measurements on pure H_2O vapor have been performed to quantify the dynamic behavior of bulk water molecules and have been carried out analogously to those of PEDOT:PSS/CNF films. [Figure 4a](#) shows the obtained susceptibility at $q = 1.5 \text{ \AA}^{-1}$ of pure H_2O vapor measured at $25 \text{ }^\circ\text{C}$.

The spectrum covers a frequency range from approximately 1 to 2500 GHz , and three individual relaxation processes can be observed. From the existing literature, these three relaxation processes can be assigned to specific hydrogen motions: at low frequencies, a diffusional process $d_{\text{H}_2\text{O}}$ is located at around 80 GHz , while at intermediate ($\approx 250 \text{ GHz}$) and high frequencies ($\approx 1300 \text{ GHz}$), an effective local process $I_{\text{H}_2\text{O}}$ and a vibrational process $\nu_{\text{H}_2\text{O}}$ appear. The diffusional process describes the translational motion of water molecules (or, more specifically, of the hydrogen atoms of the water molecules). The physical nature of the effective local process is still under debate and recently has been assigned to individual dynamics of weakly bound water molecules within the hydrogen bond net-

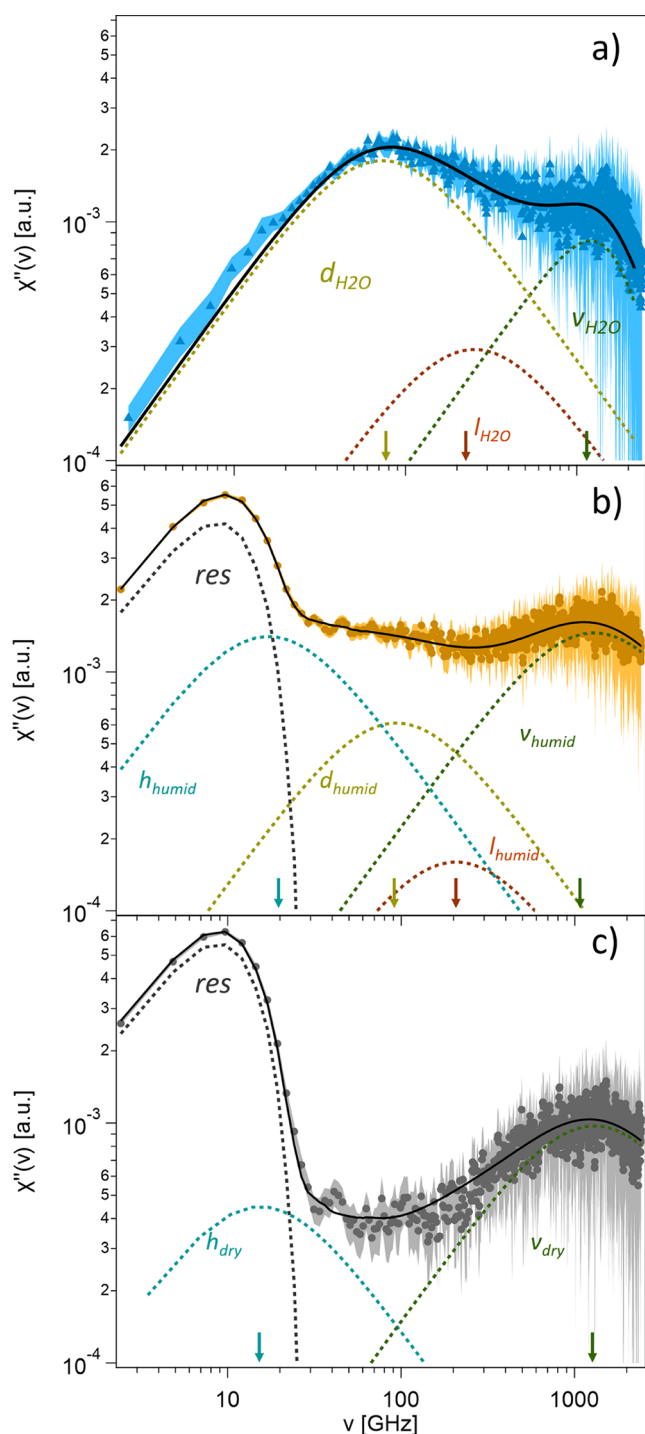


Figure 4. Dynamic susceptibilities of (a) pure H₂O and PEDOT:PSS/CNF films exposed to (b) high humidity (RH ≈ 85%) and (c) low humidity (RH ≈ 5%) measured at $q = 1.50 \text{ \AA}^{-1}$ and 25 °C. Cumulative fits according to eqs 1, 4, and 5 are shown as a full black line, while the individual contributions to the individual fitting function are shown as dashed lines: resolution function *res* (dark gray), hydration water relaxation *h* (light blue), diffusive process *d* (yellow), effective local process *l* (dark red), and a vibrational process *v* (dark green). Colored arrows indicate the respective peak positions.

work,^{45–47} while it was also proposed that this process corresponds to the rotational relaxation between quasi-equilibrium orientations of water molecules in the hydrogen bond network.^{46,48} The vibrational process has previously been

assigned to intermolecular O–O–O bending vibrations, which reflect the stiffness of the hydrogen bonding network.^{49–51} According to previous studies on water dynamics, the relaxation processes $d_{\text{H}_2\text{O}}$ and $l_{\text{H}_2\text{O}}$ can be described by a Debye function, i.e., a homogeneous relaxation process (see eq S1).⁵⁶ The Debye function includes a relaxation time τ_i and amplitude C_i , where index i stands for d or l . A damped harmonic oscillator function accounts for $v_{\text{H}_2\text{O}}$ (see ref 36 for extensive details about the analysis). The final equation used for fitting the susceptibility of pure H₂O is given by

$$\chi''_q(\nu) = \chi''_{d,\text{H}_2\text{O}}(\nu) + \chi''_{l,\text{H}_2\text{O}}(\nu) + \chi''_{v,\text{H}_2\text{O}}(\nu) \quad (1)$$

It should be noted that the frequencies of the observed relaxation processes agree very well with the literature values for liquid water.^{36,52–54} Therefore, it is likely that besides gaseous water, liquid water is also present, probably as condensate on the measurement cell walls. The diffusion of gaseous water molecules cannot be detected with QENS, since it is around 3 orders of magnitude faster than that of liquid water and would appear, e.g., in Figure 3 as flat background, indistinguishable from other background sources. Furthermore, the use of a special hollow cylinder cell strongly reduces the pathway of the incident neutrons through water vapor (see the Experimental Section for more details). Humidity measurements showed that over the course of several hours, a stable humidity of approximately 85% sets in, as can be seen in Figure S5. Therefore, the small fraction of liquid water is negligible for the QENS experiments. To further analyze the individual relaxation processes of pure H₂O, we plotted the respective relaxation times as a function of q (see Figure 5).

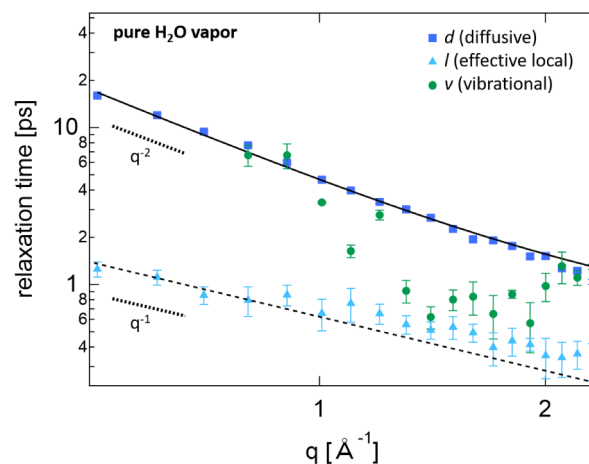


Figure 5. Relaxation times of the diffusive (blue squares), effective local (light blue triangles), and vibrational (green circles) relaxation process of pure H₂O vapor in dependence of the momentum transfer q at 25 °C. For clarity, the vibrational lifetime is shifted upward by a factor of 10^6 . The relaxation time of the diffusive process is fitted with the isotropic jump model according to eq 2, while the q^{-1} dependence is indicated by a dashed black line for the effective local process.

It can be seen that $d_{\text{H}_2\text{O}}$ features a q^{-2} dependence at low q values, while at higher q values, the slope becomes shallower. Generally, low q values correspond to larger length scales. Therefore, for dynamic processes comprising a translational component, we observe larger displacements and thus longer relaxation times of the water molecules than at high q values. Thus, the results indicate a diffusive motion on longer length

and time scales, while at shorter scales, the dynamics are increasingly affected by local motions. For the effective local relaxation process $I_{\text{H}_2\text{O}}$, roughly a q^{-1} dependence has been observed at low q values (indicated by the dashed black line), which suggests, at least partially, localized dynamic processes. For the vibrational process $\nu_{\text{H}_2\text{O}}$, appearing at higher frequencies, no q dependency was observed, but notable fluctuations, which are due to the large error bars of $\chi''(q,\nu)$ at higher frequencies, are present. Thus, $\nu_{\text{H}_2\text{O}}$ represents a purely local dynamic process compatible with intermolecular O–O–O vibrations. We want to note here that for a vibrational process, as opposed to a relaxation process, the inverse of the damping relates to the lifetime of the vibration and thus cannot be quantitatively compared with each other. Nevertheless, to point out that the vibrational process features no q dependence, we plot the data in a single figure.

Briefly summarized, the water molecules feature diffusive behavior at longer length and time scales, indicated by the q^{-2} dependency of $d_{\text{H}_2\text{O}}$. This dependency changes to a lower exponent when we observe the motion on a more local scale. There, water molecules might perform a local motion for a certain time before jumping to a new position. Such behavior can be described by the isotropic jump model.^{55–57} It should be noted that this model is strongly simplified and still under scientific debate, especially with respect to the jump mechanism. Nevertheless, it has been successfully employed to describe water diffusion under changing environmental parameters, such as temperature and pressure,^{36,52,57–59} and in films.³² Moreover, it can be used to describe the diffusion of hydration water (meaning strongly bound water) in a quantitative manner, as we show below. According to the jump-diffusion model, the q -dependent relaxation time, τ , is given by

$$\tau = \tau_0 \left[1 + \frac{6}{q^2 l_j^2} \right] \quad (2)$$

with a residence time τ_0 between the jumps and a jump length l_j . In the low q limit, a purely diffusive process can be observed, with a diffusion coefficient d given by

$$D = \frac{l_j^2}{6\tau_0} \quad (3)$$

The relaxation time of the diffusive process in pure water vapor shown in Figure 5 (blue squares) can be fitted to eq 2 to obtain a residence time τ_0 of 0.52 ps and a jump length l_j of 0.87 Å. Both values agree well with existing literature on liquid H₂O.^{36,57} By using eq 3, a diffusion coefficient of $d = (2.40 \pm 0.12) \times 10^{11} \text{ Å}^2 \text{ s}^{-1}$ is obtained. Also, the diffusion coefficient agrees very well with reported values for liquid water (approximately $(2.3\text{--}2.6) \times 10^{11} \text{ Å}^2 \text{ s}^{-1}$).^{36,52–54} This underlines our earlier assumption that besides gaseous water, a certain fraction of liquid water is present, most likely as a condensate on the measurement cell walls.

Water Dynamics in PEDOT:PSS/CNF Films. The dynamic properties of water inside PEDOT:PSS/CNF films were measured under the same experimental conditions as those for pure H₂O vapor. The presence of small fractions of liquid water, as was found in the QENS measurements of pure H₂O vapor, is negligible for the absorption behavior of the PEDOT:PSS/CNF film.¹⁹ From earlier work, we can deduce

that the PEDOT:PSS/CNF films absorb approximately 24 vol % of water in humid environment, based on our data in ref 19. This has been calculated by comparing the neutron scattering length densities of the PEDOT:PSS/CNF films in a dry and humid water environment. This is a common routine to obtain the absorbed water content.^{34,35} More information can be found in the Supporting Information. A swelling process was not observed for the PEDOT:PSS/CNF films. It should be mentioned that these films featured a thickness of around 100 nm and, thus, were significantly thinner than the films used in this work, which are around 10 μm in thickness. Hence, the exact same absorption behavior with respect of the final water content cannot be assumed, as interface effects are less pronounced in thicker PEDOT:PSS/CNF films. Nevertheless, the calculated value of 24 vol % provides a good estimation of the absorbed water content and proves that water is absorbed into the films and thus, is in the vicinity of PEDOT:PSS/CNF. Therefore, water–polymer interactions become relevant. In the following, we will analyze $\chi''(q,\nu)$ of the PEDOT:PSS/CNF films under low and high humidity during the first cycle, before we discuss the reproducibility of the obtained results during the subsequent two cycles. Figure 4b shows $\chi''(q,\nu)$ of the PEDOT:PSS/CNF film exposed to high humidity during the first cycle. The differences from pure H₂O vapor (Figure 4a) are clearly evident. A pronounced peak at low frequencies (below 10 GHz) indicates the presence of slow-moving moieties. Since the peak approaches the elastic line, which gives the resolution limit of the INS instrument, we decided to include it in the deconvolution of $\chi''(q,\nu)$ to model dynamics that are too slow to be resolved. Consequently, this peak is denoted as res (in some publications this peak is also denoted as elastic fraction, el). The amplitude is varied within the fits, as has already been confirmed in previous studies to be a suited procedure.^{36,44} In addition, the HWHM of the instrument resolution function, which amounts to 8 GHz, is considered. While the elastic line is included into the fitting function, its amplitude and position are not interpreted. For interpretation of the results, only data that lie above this HWHM is used. At intermediate frequencies (from 25 to 300 GHz), the susceptibility decreases into a plateau before another peak at higher frequencies appears (≈ 1300 GHz). To model $\chi''(q,\nu)$, four individual relaxation processes and the elastic fraction, overlaid by the instrument resolution function, are summed. In addition to the three peaks already observed for pure H₂O vapor (diffusive $d_{\text{H}_2\text{O}}$, effective local $I_{\text{H}_2\text{O}}$, and vibrational $\nu_{\text{H}_2\text{O}}$ process), another relaxation process appears at a very low frequency (≈ 20 GHz). This is still well above the HWHM of the resolution function, and is, therefore, considered for the following analysis. As was already explained earlier, we assign the peak to the diffusion of strongly bound and thus slowly moving hydration water, labeled as h_{humid} . The other dynamical relaxations, d_{humid} , l_{humid} , and ν_{humid} , appear at different frequencies as compared to the respective positions that have been observed for pure H₂O: $d_{\text{humid}} \approx 94$ GHz ($d_{\text{H}_2\text{O}} \approx 80$ GHz), $l_{\text{humid}} \approx 210$ GHz ($I_{\text{H}_2\text{O}} \approx 250$ GHz), and $\nu_{\text{humid}} \approx 1250$ GHz ($\nu_{\text{H}_2\text{O}} \approx 1300$ GHz). These changes refer to the presence of PEDOT:PSS/CNF, which interacts with the water molecules and affects the diffusive water behavior as well as the localized motions (l) and vibrations (ν) of the water molecules. Analogous to pure H₂O, d_{humid} and l_{humid} are described with a Debye function, while for ν_{humid} a damped harmonic oscillator function is used. The relaxation of

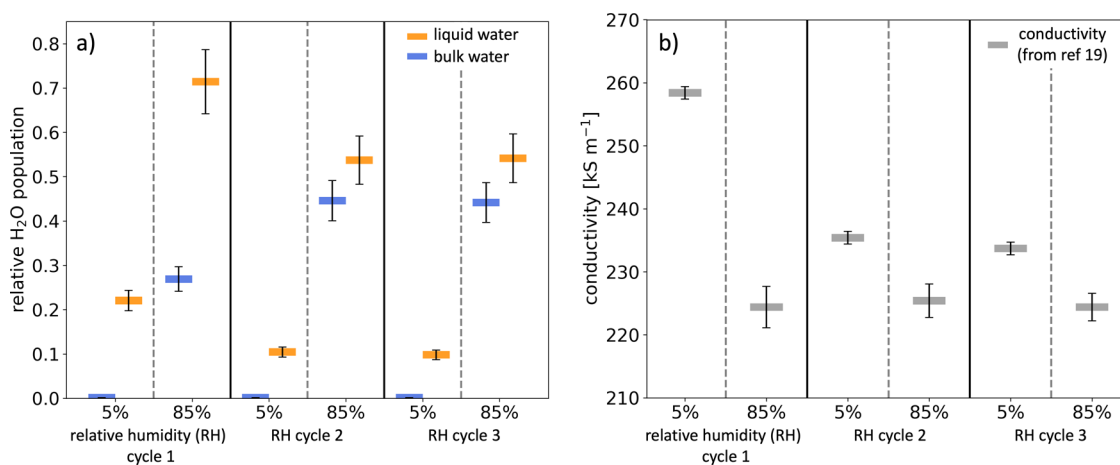


Figure 6. (a) Relative populations of bulk (blue) and hydration water (orange) and (b) electrical conductivity of the PEDOT:PSS/CNF films during three cycles of exposure to low and high humidity. The population of hydration water in a low-humidity environment is relative to the humid states. The conductivity data have been taken from ref 19.

hydration water h_{humid} is addressed analogously to the diffusive relaxation of bulk water d_{humid} with a Debye function. In summary, $\chi''(q, \nu)$ of the PEDOT:PSS/CNF films in a humid environment is modeled with the following equation:

$$\chi''_q(\nu) = \chi''_{\text{res, humid}}(\nu) + \chi''_{h, \text{humid}}(\nu) + \chi''_{d, \text{humid}}(\nu) + \chi''_{l, \text{humid}}(\nu) + \chi''_{v, \text{humid}}(\nu) \quad (4)$$

For the PEDOT:PSS/CNF films in a dry environment, the water dynamics are markedly different (Figure 4c): overall, $\chi''_q(\nu)$ is much lower, confirming that less water is present in the film. In addition, the contributions of bulk water, d_{humid} and the local effective process, h_{humid} , are not required to satisfactorily model $\chi''_q(\nu)$. Thus, this is a strong hint that bulk water is completely released from the PEDOT:PSS/CNF film. In contrast, the contribution of hydration water, h_{dry} is still present, albeit with a smaller amplitude, meaning that even in a dry environment, a certain amount of hydration water remains within the film. This is even the case for pure CNF thin films.⁶⁰ Furthermore, its frequency is lowered ($h_{\text{dry}} \approx 10$ GHz) as compared to the hydration water in the humid state ($h_{\text{humid}} \approx 20$ GHz), which indicates a further slow-down of the hydration water dynamics, and thus on average a stronger binding with PEDOT:PSS/CNF. In addition, contributions from the vibrational process, ν_{dry} analogous to the susceptibility of the film in a humid state, are still present but located at different frequencies: $\nu_{\text{dry}} \approx 1350$ GHz ($\nu_{\text{humid}} \approx 1250$ GHz). Apparently, the changes in the hydration layer, due to the partial release of hydration water, lead to a certain rearrangement of water molecules reflected in the shifts of the frequency of the vibrational process, ν_{dry} . This is probably due to the release of water molecules from the hydrophobic groups of PEDOT:PSS/CNF, primarily driven by entropic effects and an entropic gain. In contrast, the hydrophilic groups remain hydrated via hydrogen bonds, even in a dry environment. Therefore, the function used to model $\chi''_q(\nu)$ of the PEDOT:PSS/CNF films in a dry environment consists of the following contributions:

$$\chi''_q(\nu) = \chi''_{\text{res, dry}}(\nu) + \chi''_{h, \text{dry}}(\nu) + \chi''_{v, \text{dry}}(\nu) \quad (5)$$

Briefly summarized from the susceptibility data during the first cycle of exposure to low and high humidity, the following picture emerges: under high humidity conditions, H₂O is present in gaseous and, to a small extent, also in liquid form around the PEDOT:PSS/CNF film. In addition, we observe water absorption into the film, where two different water species, bulk and hydration water, are present. Hydration water is strongly bound to PEDOT:PSS/CNF, which therefore diffuses significantly slower than freely moving bulk water. When the ambient relative humidity is decreased, all bulk water and parts of the hydration water are released from the film. As a result, the relaxation of the diffusive process of the hydration water shifts to lower frequencies; i.e., the hydration water dynamics become even slower. This means that, on average, the binding between the remaining hydration water and PEDOT:PSS/CNF becomes stronger. We hypothesize that hydration water around hydrophobic groups leaves the film, leading to an entropy gain, while strongly bound water around hydrophilic groups remains and retains its binding strength. Also, the vibrational ν_{dry} relaxation processes feature a shift in frequency. While this shift is weak, it still highlights that the structure of the hydration layer and its orientation around PEDOT:PSS/CNF depend on the ambient humidity. In the following, we focus on a quantitative analysis of the relaxation processes of hydration and bulk water within all three cycles of exposure of the PEDOT:PSS/CNF films to low and high humidity.

Relative Populations of Hydration and Bulk Water.

The amplitudes of the relaxation processes of susceptibility are proportional to the respective scattering intensities. Thus, the relative populations of bulk and hydration water can be determined as follows:

$$f_i = \frac{C_i}{C_h + C_d} \quad (6)$$

Here, i stands for d or h , i.e., the fraction of bulk or hydration water, respectively. For the determination of the relative populations of the water species, averaged values of the amplitudes C_i from QENS measurements at momentum transfer $q = 1.4, 1.5,$ and 1.6 \AA^{-1} were used. The effective local relaxation l process is not included in the calculations as it is most likely coupled to the diffusive process d of bulk water,

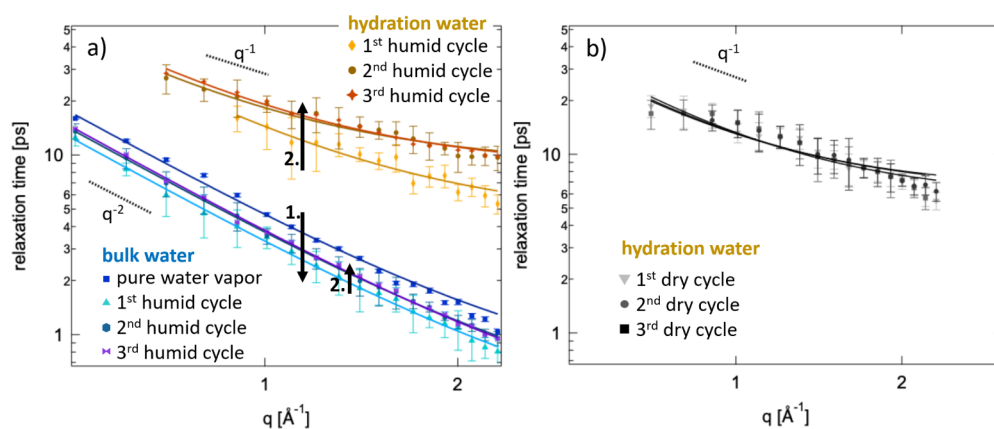


Figure 7. Relaxation times of the bulk (blue colors) and hydration water (orange and gray colors for the (a) humid and (b) dry states, respectively) throughout the (a) humid and (b) dry states as a function of momentum transfer q at 25 °C. In addition, the relaxation times of the diffusive process of pure H₂O are shown (dark blue squares). The full lines represent fits of the isotropic jump model according to eq 2. The black arrows in (a) indicate (1) the decrease in relaxation times with respect to the diffusive relaxation of pure H₂O and bulk water within the PEDOT:PSS/CNF film and (2) the increase in relaxation time after the first cycle.

i.e., bulk water molecules contribute to both d and l . Neither are the vibrational processes included, as both water species might contribute to those. The elastic fraction that is represented within the resolution function, res , is also not considered. Figure 6a shows the resulting relative populations of the bulk (blue) and hydration water (orange) throughout the three cycles of exposure to low and high humidity.

Throughout all three cycles, more hydration water than bulk water is present inside the PEDOT:PSS/CNF films. This is consistent with the observation that the films feature no swelling, despite a water uptake of approximately 24 vol %.¹⁹ This is due to the CNFs, which significantly enhance the mechanical integrity of the pure PEDOT:PSS film.⁴ Their stiffness keeps the PEDOT:PSS clusters in place, which consequently minimizes the creation of available space between them. Thus, the uptake of bulk water is limited, and swelling is prevented. Furthermore, good reproducibility is observed regarding the uptake and release of both water species in the second and third cycles, whereas the first cycle slightly differs with respect to the second and third cycles. In the first cycle, a larger amount of hydration water and a smaller amount of bulk water are found. Such behavior, where the first cycle differs from the subsequent ones, has also been found regarding the nanostructure of the PEDOT:PSS/CNF film.^{19,61} During the first swelling cycle, irreversible structural rearrangements occurred, while upon switching between dry and humid states, a reproducible change in nanostructure was found. Thus, the PEDOT:PSS/CNF film morphology is directly correlated with the occurring water dynamics, which eventually also affects the electrical conductivity. For a better understanding, we show the conductivity data originally reported in ref 19 in Figure 6b. Altogether, the following scenario can be sketched, for visualization of the structural model, which is described in the following, please see Figure 1 in ref 19: during spray deposition of the aqueous PEDOT:PSS/CNF solution onto a heated Si substrate (110 °C), the excess water quickly evaporates. The evaporation rate of water is faster than the structural equilibration of the PEDOT:PSS/CNF nanocomposite, which results in a kinetically trapped film morphology, where CNF bundles as well as individual CNFs are covered with PEDOT:PSS.⁶¹ Larger PEDOT:PSS-rich domains are present between the CNFs.^{19,61}

Despite the low humidity, this morphology allows the PEDOT:PSS/CNF film to host a certain fraction of hydration water, which is known to play a crucial role in polymer chain mobility: upon humidification, the amount of hydration water increases significantly, thereby increasing the polymer chain mobility. Bulk water is absorbed into the film as well. Eventually, the large amount of absorbed water allows the film to escape the kinetically trapped film morphology. During the following structural rearrangements, PEDOT:PSS dewets from the CNF surface and forms smaller clusters. As a consequence, the conductivity decreases. Upon drying, all bulk water and parts of the hydration water are released from the film. This leads to the formation of large CNF bundles, but also to a rewetting of these CNF bundles with PEDOT:PSS. Consequently, the electrical conductivity increased. In addition, PEDOT:PSS-rich domains, which are larger than the domains found in the initial dry state, are present. The described structural rearrangements that occur during the first cycle are irreversible. In the subsequent two cycles, we see further structural changes when switching between a dry and humid environment, which are reversible.¹⁹ In these states, the hydration layer around PEDOT:PSS and CNFs contains fewer water molecules compared to the first cycle, while more bulk water is present. This suggests that during the irreversible structural changes, more available space within the PEDOT:PSS/CNF film is created, which, under humid conditions, is then occupied by bulk water.

Generally, a larger amount of hydration and bulk water leads to a dewetting of the PEDOT:PSS from the CNF bundles and, thus, to a lower electrical conductivity (see Figure 6). However, the highest conductivity was observed in the dry state of the first cycle, where an increased amount of hydration water compared to the subsequent dry states is present. Whether this is due to an initial structure, which irreversibly changes later on, or to the presence of hydration water that is especially beneficial for the wetting of PEDOT:PSS on the CNFs and conductive properties remains an open question. A study that focuses on the selective tuning of the hydration water amount, e.g., by temperature, additives, and chemical modification of PEDOT:PSS/CNF, and how this impact conductivity, is currently ongoing.

Relaxation Times of Bulk and Hydration Water. The q dependence of the relaxation times of bulk and hydration water contains information about the nature of their diffusive behavior. Figure 7 shows the respective relaxation times of bulk and hydration water as a function of q during the three cycles of exposure to high (Figure 7a) and low humidity (Figure 7b). In addition, the relaxation time obtained from the QENS measurement on pure H₂O is plotted in Figure 7a.

For the bulk water, a nearly perfect q^{-2} dependency is found at large q values, which represents a purely diffusive process. With increasing q , the dependency becomes slightly weaker, which is due to the stronger effect of local motions, as explained above. Interestingly, the relaxation times of pure H₂O are slightly larger than those of bulk water in the PEDOT:PSS/CNF films (indicated with a black arrow labeled 1 in Figure 7a). Thus, the presence of the polymers leads to an acceleration of the bulk water diffusion. This might be due to long-range interactions of the PEDOT:PSS/CNF material that reach beyond the hydration layer and also affect the diffusion of bulk water. However, we can only speculate about the origin of such interactions. In contrast, the relaxation times of the diffusive process of hydration water in the humid and dry states (h_{humid} and h_{dry}) feature a q^{-1} dependency, which indicates more localized dynamics. This makes sense, as the hydrogen bonds between hydration water and the hydrophilic groups of PEDOT:PSS/CNF are stronger than those between bulk water molecules. Lateral diffusion analogous to bulk water is, therefore, hindered. In addition, a longer relaxation time as compared to that of the diffusion process of bulk water was found. The q^{-1} dependency becomes even shallower with increasing q . In addition, for both water species, a shorter relaxation time was observed during the first humid and dry state, whereas in the subsequent two cycles, the relaxation times increased. In Figure 7, this is marked with two black arrows labeled 2. We relate this observation to structural rearrangements as was explained earlier. Similar to the analysis of pure H₂O, we again use the isotropic jump model according to eq 2 for the analysis of the hydration and bulk water. From this model, we can extract the jump length l_j and residence time τ_0 , which are shown as a function of relative humidity in Figure 8.

Generally, reproducible behavior is observed in the second and third cycles, whereas the first cycle differs slightly. This is attributed to the initial change in the PEDOT:PSS/CNF morphology and the dynamic structure of the hydration layer in the first cycle, as was discussed earlier. For hydration water, the residence times are longer in the dry state as compared to those in the humid state. This is probably due to the release of hydration water around hydrophobic groups, while water molecules that are strongly bound via hydrogen bonds to hydrophilic groups remain in the films. The respective jump lengths are similar in the dry and humid states. In contrast, bulk water is able to move more freely within the films, which is reflected by its very short jump lengths and residence times. Notably, the found values for τ_0 and l_j are similar to those of pure water. Compared to other polymeric systems, such as poly(*N*-isopropylacrylamide) in aqueous solution, the jump lengths and residence times of bulk water are comparable.³⁶ However, the values obtained for hydration water in this study are higher, suggesting stronger hydrogen bonds. Another study about the water transport mechanism in polymeric membranes obtains much higher residence times and jump lengths as compared to our study.⁶² It is important to note that such

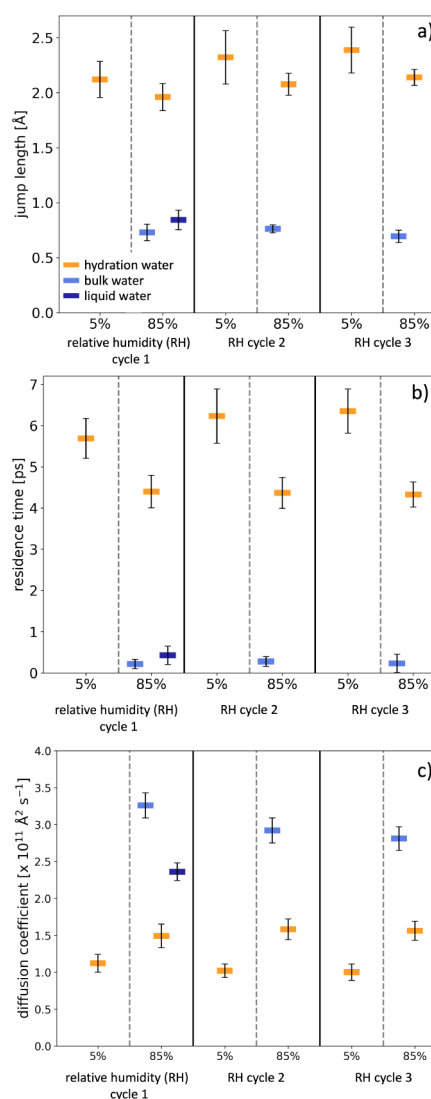


Figure 8. (a) Jump length l_j , (b) residence time τ_0 , and (c) diffusion coefficient as functions of relative humidity for hydration (orange) and bulk water (blue). The values have been obtained by fitting the isotropic jump model, according to eq 2, to the q -dependent relaxation times. Please note that during exposure to low humidity, bulk water is released from the PEDOT:PSS/CNF film completely, and hence, no data points are obtained. The corresponding values for liquid H₂O are shown in dark blue.

values are challenging to compare directly, as residence times and jump lengths depend on various factors, including polymer concentration, the specific nature of the polymer (e.g., ratio of hydrophilic and hydrophobic groups), and the temperature. For the two water species, the diffusion coefficients can be calculated following eq 3. As already discussed, we obtain a slightly higher diffusion coefficient for bulk water inside the PEDOT:PSS/CNF film (around $3 \times 10^{11} \text{Å}^2 \text{s}^{-1}$, see Figure 8c) as compared to pure H₂O ($2.40 \pm 0.12 \times 10^{11} \text{Å}^2 \text{s}^{-1}$). Thus, the diffusion of bulk water is faster inside the film than in pure water, which may be due to long-range interactions with the PEDOT:PSS/CNF. In contrast, the average diffusion coefficient of hydration water is significantly lower. Analogous to the residence time, the diffusion coefficient of hydration water is even slower in dry environments. As discussed above, this is presumably due to the release of water molecules from around hydrophobic groups, whereas the binding strengths of

water molecules toward hydrophilic groups are sufficiently strong to keep these water molecules within the film, even in a dry environment. As a result, the average diffusion coefficient obtained via QENS is smaller. Despite the detailed analysis, open questions still remain: how many water molecules form the hydration layer? How are the water dynamics and thus the structure affected by surface charges of the CNF and the respective counterion concentration? How does the water behavior differ depending on whether a water molecule is in the vicinity of a PEDOT:PSS chain or CNF bundle? The details obtained here, in particular from the isotropic jump-diffusion model, provide valuable input for numerical simulations that can contribute to the above-raised questions and therefore allow for an even deeper understanding of the relationship between structure, dynamics, and conductivity in complex conductive nanocomposite polymer films.

CONCLUSION

We investigated the dynamic behavior of water in PEDOT:PSS/CNF films that were exposed to three cycles of low and high humidity. For this, quasi-elastic neutron scattering (QENS) was used. To better differentiate between the individual relaxation processes, the obtained dynamical structure factors were transformed to the imaginary part of the dynamic susceptibility. We identified dynamic relaxation processes of two different water species: fast-moving bulk water and slow-moving hydration water. In a humid environment, both species are present within the film, while, upon drying, bulk water is released completely. In contrast, hydration water is always present to a certain extent, even in a dry state. During the first cycle of exposing the PEDOT:PSS/CNF film to low and high humidity, the fraction of hydration water is larger as compared to the following two cycles. This is attributed to a changing film morphology: the PEDOT:PSS/CNF solution has been spray-coated onto a heated Si-substrate, which leads to fast water evaporation. Apparently, this evaporation rate is faster than the structural equilibration of the PEDOT:PSS/CNF film, resulting in a kinetically trapped film morphology, which is able to host a larger fraction of hydration water as compared to the later equilibrated film morphology. In turn, this leads to enhanced mobility of the PEDOT:PSS/CNFs and eventually allows the film to escape the kinetically trapped film morphology. As the following cycles feature a smaller amount of hydration water but a larger amount of bulk water, we conclude that these initial rearrangements are irreversible. In contrast, a reproducible amount of hydration and bulk water was observed during the subsequent humid and dry states, which indicates reversible structural rearrangements. This agrees very well with a recent study on the structural properties of the PEDOT:PSS/CNF films.¹⁹

The QENS measurements and the subsequent analysis of $\chi''(q, \nu)$ provide a detailed picture of the water dynamics inside the PEDOT:PSS/CNF films. By correlating the dynamical properties to the film morphology, the role of hydration and bulk water during the occurring structural rearrangements upon changing relative humidity is resolved, while also the impact of both water dynamics and film morphology on the electrical conductivity was investigated. In a dry environment, bulk water is completely absent in the film, whereas parts of the hydration water remain in the film, preferably around the hydrophilic groups of PEDOT:PSS/CNF. As a result, the CNF bundles are covered by PEDOT:PSS, which eventually leads to

an increased conductivity. By exposing the PEDOT:PSS/CNF films to a humid environment, both bulk and hydration water are present in the film, with more hydration than bulk water. This is attributed to the enhanced mechanical stability of the films due to the CNFs, which limits water uptake and prevents a swelling process compared to pure PEDOT:PSS.⁴ Consequently, upon humidifying the environment, little open space within the PEDOT:PSS/CNF film is created that can be occupied by bulk water. More hydration water is present around PEDOT:PSS and CNF, while it is also more strongly bound. As a consequence, PEDOT:PSS dewets from the CNF bundles, and the conductivity decreases. We demonstrated that the water dynamics are closely correlated to the structural and conductive properties of PEDOT:PSS/CNF films.

By tuning the interactions between water and PEDOT:PSS and CNFs, e.g., by temperature, salt additives, or chemical modification of the polymers, the film morphology and, thus, the conductivity might be further optimized. In addition, the detailed information about the diffusive behavior of both water species inside the PEDOT:PSS/CNF films serves as input for molecular dynamics simulations to further deepen our understanding of the dynamics-structure-performance relationship.

EXPERIMENTAL SECTION

Materials. PEDOT:PSS was purchased from Sigma-Aldrich and used as received. 2,2,6,6-Tetramethylpiperidine-1-oxyl (TEMPO) oxidized cellulose nanofibrils (CNFs) gel was prepared by using the protocol of Isogai et al.¹² Deionized H₂O was used from a Milli-Q setup. D₂O was kindly provided by the Institut Laue-Langevin.

Preparation of PEDOT:PSS/CNF Films Using Spray Ink Deposition. 2,2,6,6-Tetramethylpiperidine-1-oxyl (TEMPO) oxidized cellulose nanofibrils (CNFs) gel was dispersed in ultrapure water via mechanical mixing and sonification (each for 10 min) to a concentration of 0.03 wt %. After that, the CNF dispersion was centrifuged for 60 min at 4800 rpm. The final CNFs had diameters of roughly 4 nm. The carboxylate content was 800 $\mu\text{mol g}^{-1}$. For the preparation of the PEDOT:PSS/CNF ink, PEDOT:PSS (1.1% in H₂O) was mixed with the CNF dispersion in a volume ratio of 1:1 and stirred overnight.

Subsequently, the PEDOT:PSS/CNF films were sprayed layer-by-layer by using a nozzle (Compact JAU D555000, Spray Systems Inc.) attached to a motorized linear stage (LTS300/M, Thorlabs Inc.). The spray-coating setup allows the fabrication of films on a larger scale and thus is also of industrial relevance. The used carrier gas was nitrogen, and the spray pressure was set to 1 bar. The sample-to-nozzle distance was kept constant at 20 cm. The substrate was heated to 110 °C to minimize coffee ring effects and accelerate the fabrication process. The flow rate was kept constant at 6.5 L min⁻¹. The first 20 layers were sprayed layer-by-layer with a drying time of 20 s in between each layer. After that, 25 double layers were deposited with a drying time of 20 s between each deposited double layer. After the samples cooled down, they were carefully peeled off from the substrate with the help of sharp plastic tweezers.

Optical and Atomic Force Microscopy. A digital microscope (Keyence Corporation, VHX-X1 series, Japan) was used for microscopy measurements, applying a magnification of 2500. For atomic force microscope (AFM) measurements, a Bruker MultiMode 8 in ScanAsyst mode was used. The samples were probed using a nitride lever (T: 650 nm; L: 115 nm; f: 70 kHz; model ScanAsyst-air) with an Al-coated silicon tip. The scan rate was set to 0.501 Hz. The roughness was calculated based on $1 \times 1 \mu\text{m}^2$ large images using the software Gwyddion (v2.56).⁶³

Scanning Electron Microscopy. For scanning electron microscopy (SEM) measurements, a ZEISS Crossbeam 550L FE-SEM instrument with a SESI detector was used. Prior to the measurements, the samples were coated with a 4-nm thin gold layer via sputtering at a

current of 2.2 mA and a pressure of 100 mbar for 12 s. The acceleration voltage was set to 3 kV at a working distance of 4–5 mm.

Quasi-Elastic Neutron Scattering (QENS). QENS measurements⁶⁴ were conducted at the cold time-of-flight spectrometer IN5 at the ILL, Grenoble, France.⁶⁵ The incident neutrons had a wavelength of 5 Å. The rotation speed of the chopper system was set to 12,000 rpm. This combination results in an elastic energy resolution of 77 μeV (fwhm) and energy transfer of -10 to 2.5 meV. Thus, the measurements were performed on the energy-loss side. The free-standing PEDOT:PSS films had a film thickness of $10 \pm 1 \mu\text{m}$ and measured approximately 7 cm in length and 1.5 cm in width (please see also Figure S4). Two of these films (with a small overlap at their long sides) were rolled around the inner aluminum cylinder of a standard hollow cylinder cell provided by the IN5 instrument. Aluminum foil was used to hold the films in position, and the inner aluminum cylinder was mounted within the outer part of the hollow cylinder cell. For QENS measurements under dry conditions, the entire cell was flushed with nitrogen for 15 min, while for QENS measurements in a humid environment, 20 μL of deionized H_2O or D_2O , respectively, was added into the outer part of the hollow cylinder cell before connecting it with the inner part. This amount of water might seem small; however, given the very narrow space between the inner and outer cylinder wall of 0.1 mm, 20 μL was sufficient for humidifying the surrounding films. A graph that shows the temporal evolution of the relative humidity (H_2O and D_2O) inside the cylinder cell is provided in the Supporting Information. Afterward, the hollow cylinder cell was closed using 16 screws. The films in a dry state were measured directly afterward, whereas the films in a humid state were equilibrated in the saturated water atmosphere (relative humidity of approximately 85%) for 3 h. Thus, one full cycle consists of drying via nitrogen, collecting the data of the dry PEDOT:PSS/CNF film, hydrating the film by adding 20 μL of water into the cylinder cell, and collecting the data of the humid PEDOT:PSS/CNF film after an equilibration time of 3 h. Overall, this procedure was repeated three times.

Overall, we performed two individual experiments, each consisting of three cycles of exposure to dry and humid environments, as described above. During Experiment A, we used H_2O , while in Experiment B, we used D_2O for humidifying the films' surroundings. In this way, the scattering signal will be dominated by the incoherent scattering originating from hydrogen atoms of either H_2O molecules (Experiment A) or PEDOT:PSS/CNFs (Experiment B), respectively. From reference Experiment B, we can be sure to detect mainly water dynamics with QENS. For more information about Experiment B, please see the Supporting Information. The general measurement protocol is schematically shown in Figure 2. Measurement time for each QENS spectrum was 2.5 h. The scattering signal was recorded by He^3 detector tubes covering a q range from 0.5 to 2.3 \AA^{-1} . The obtained spectra were normalized to the incoming neutron flux and a vanadium standard measurement. In addition, we performed empty cell measurements (in dry and humid (H_2O and D_2O) states) for background corrections. Eventually, the software Mantid was used to convert the time-of-flight data to energy transfers of the neutrons and to bin the resulting spectra in groups of equal Δq .⁶⁶ The obtained dynamic structure factor $S(q, \Delta E)$ was then transformed into the susceptibility $\chi''(\nu)$ as explained in the main text and ref 36.

■ ASSOCIATED CONTENT

SI Supporting Information

The Supporting Information is available free of charge at <https://pubs.acs.org/doi/10.1021/acs.macromol.4c02412>.

The characterization of the PEDOT:PSS/CNF films with optical microscopy, atomic force microscopy, and scanning electron microscopy, as well as a photograph of the free-standing PEDOT:PSS/CNF films, along with details about how the PEDOT:PSS/CNF films were mounted within the QENS sample cells; in addition, the evolution of the relative humidity within the sample cells

used for QENS measurements is shown; we also show the susceptibility of the PEDOT:PSS/CNF film in humid D_2O vapor, the Debye function used for fitting the susceptibility, and the calculation of the water content of the PEDOT:PSS/CNF films in humid water vapor; we provide details for the evolution of the susceptibility fit upon adding the individual dynamic processes; all measured dynamic structure factors $S(q, \Delta E)$ are shown (PDF)

■ AUTHOR INFORMATION

Corresponding Author

Lucas P. Kreuzer – Heinz Maier-Leibnitz-Zentrum, Technische Universität München, Garching 85748, Germany; orcid.org/0000-0002-9669-2130; Email: lucas.kreuzer@frm2.tum.de

Authors

Marie Betker – Deutsches Elektronen Synchrotron DESY, Hamburg 22607, Germany

Marcell Wolf – Heinz Maier-Leibnitz-Zentrum, Technische Universität München, Garching 85748, Germany

Bart-Jan Niebuur – INM - Leibniz-Institute for New Materials, Saarbrücken 66123, Germany; orcid.org/0000-0003-1422-3996

Jacques Ollivier – Institut Laue-Langevin, Grenoble 38000, France

L. Daniel Söderberg – Department of Fibre and Polymer Technology, KTH Royal Institute of Technology, Stockholm 100 44, Sweden; Wallenberg Wood Science Center, Royal Institute of Technology KTH, Stockholm 100 44, Sweden; orcid.org/0000-0003-3737-0091

Stephan V. Roth – Deutsches Elektronen Synchrotron DESY, Hamburg 22607, Germany; Department of Fibre and Polymer Technology, KTH Royal Institute of Technology, Stockholm 100 44, Sweden; Wallenberg Wood Science Center, Royal Institute of Technology KTH, Stockholm 100 44, Sweden

Complete contact information is available at:

<https://pubs.acs.org/10.1021/acs.macromol.4c02412>

Notes

The authors declare no competing financial interest.

■ ACKNOWLEDGMENTS

The authors thank the ILL and especially the staff of IN5 for their excellent support before, during, and after the QENS measurements. Neutron scattering data are available at 10.5291/ILL-DATA.9-11-2126.

■ REFERENCES

- (1) Sun, K.; Zhang, S.; Li, P.; Xia, Y.; Zhang, X.; Du, D.; Isikgor, F. H.; Ouyang, J. Review on application of PEDOTs and PEDOT: PSS in energy conversion and storage devices. *J. Mater. Sci.: Mater. Electron.* **2015**, *26*, 4438–4462.
- (2) Fan, X.; Nie, W.; Tsai, H.; Wang, N.; Huang, H.; Cheng, Y.; Wen, R.; Ma, L.; Yan, F.; Xia, Y. PEDOT: PSS for Flexible and Stretchable Electronics: Modifications, Strategies, and Applications. *Adv. Sci.* **2019**, *6*, 1900813.
- (3) Tseghai, G. B.; Mengistie, D. A.; Malengier, B.; Fante, K. A.; Van Langenhove, L. PEDOT: PSS-Based Conductive Textiles and Their Applications. *Sensors* **2020**, *20*, 1881.

- (4) Bießmann, L.; Kreuzer, L. P.; Widmann, T.; Hohn, N.; Moulin, J.-F.; Müller-Buschbaum, P. Monitoring the Swelling Behavior of PEDOT: PSS Electrodes under High Humidity Conditions. *ACS Appl. Mater. Interfaces* **2018**, *10*, 9865–9872.
- (5) Zhanshayeva, L.; Favaron, V.; Lubineau, G. Macroscopic Modeling of Water Uptake Behavior of PEDOT: PSS Films. *ACS Omega* **2019**, *4*, 21883–21890.
- (6) Ko, K.-J.; Lee, H. B.; Kang, J.-W. Flexible, Wearable Organic Light-Emitting Fibers Based on PEDOT: PSS/Ag-Fiber Embedded Hybrid Electrodes for Large-Area Textile Lighting. *Adv. Mater. Technol.* **2020**, *5*, 2000168.
- (7) Fischer, R.; Gregori, A.; Sahakalkan, S.; Hartmann, D.; Büchele, P.; Tedde, S. F.; Schmidt, O. Stable and highly conductive carbon nanotube enhanced PEDOT: PSS as transparent electrode for flexible electronics. *Org. Electron.* **2018**, *62*, 351–356.
- (8) Sarabia-Riquelme, R.; Andrews, R.; Anthony, J. E.; Weisenberger, M. C. Highly conductive wet-spun PEDOT: PSS fibers for applications in electronic textiles. *J. Mater. Chem. C* **2020**, *8*, 11618–11630.
- (9) Chen, H.; Xu, H.; Luo, M.; Wang, W.; Qing, X.; Lu, Y.; Liu, Q.; Yang, L.; Zhong, W.; Li, M.; Wang, D. Highly Conductive, Ultrastrong, and Flexible Wet-Spun PEDOT: PSS/Ionic Liquid Fibers for Wearable Electronics. *ACS Appl. Mater. Interfaces* **2023**, *15*, 20346–20357.
- (10) Oesef, K.; Cranston, E. D.; Abdin, Y. Current advances in processing and modification of cellulose nanofibrils for high-performance composite applications. *Mater. Des.* **2024**, *247*, 113417.
- (11) Eichhorn, S. J.; et al. Current international research into cellulose as a functional nanomaterial for advanced applications. *J. Mater. Sci.* **2022**, *57*, 5697–5767.
- (12) Isogai, A.; Saito, T.; Fukuzumi, H. TEMPO-oxidized cellulose nanofibers. *Nanoscale* **2011**, *3*, 71–85.
- (13) Xu, X.; Liu, F.; Jiang, L.; Zhu, J. Y.; Haagensohn, D.; Wiesenborn, D. P. Cellulose Nanocrystals vs. Cellulose Nanofibrils: A Comparative Study on Their Microstructures and Effects as Polymer Reinforcing Agents. *ACS Appl. Mater. Interfaces* **2013**, *5*, 2999–3009.
- (14) Mittal, N.; Ansari, F.; Gowda, K.; Brouzet, C.; Chen, P.; Larsson, P. T.; Roth, S. V.; Lundell, F.; Wågberg, L.; Kotov, N. A.; et al. Multiscale Control of Nanocellulose Assembly: Transferring Remarkable Nanoscale Fibril Mechanics to Macroscale Fibers. *ACS Nano* **2018**, *12*, 6378–6388.
- (15) Hamed, M. M.; Ainla, A.; Güder, F.; Christodouleas, D. C.; Fernández-Abedul, M. T.; Whitesides, G. M. Integrating Electronics and Microfluidics on Paper. *Adv. Mater.* **2016**, *28*, 5054–5063.
- (16) Malti, A.; Edberg, J.; Granberg, H.; Khan, Z. U.; Andreasen, J. W.; Liu, X.; Zhao, D.; Zhang, H.; Yao, Y.; Brill, J. W.; et al. An Organic Mixed Ion–Electron Conductor for Power Electronics. *Adv. Sci.* **2016**, *3*, 1500305.
- (17) Edberg, J.; Malti, A.; Granberg, H.; Hamed, M. M.; Crispin, X.; Engquist, I.; Berggren, M. Electrochemical circuits from ‘cut and stick’ PEDOT: PSS-nanocellulose composite. *Flexible Printed Electron.* **2017**, *2*, 045010.
- (18) Gåremark, J.; Yang, X.; Sheng, X.; Cheung, O.; Sun, L.; Berglund, L. A.; Li, Y. Top-Down Approach Making Anisotropic Cellulose Aerogels as Universal Substrates for Multifunctionalization. *ACS Nano* **2020**, *14*, 7111–7120.
- (19) Brett, C. J.; Forslund, O. K.; Nocerino, E.; Kreuzer, L. P.; Widmann, T.; Porcar, L.; Yamada, N. L.; Matsubara, N.; Månsson, M.; Müller-Buschbaum, P.; et al. Humidity-Induced Nanoscale Restructuring in PEDOT: PSS and Cellulose Nanofibrils Reinforced Biobased Organic Electronics. *Adv. Electron. Mater.* **2021**, *7*, 2100137.
- (20) Bellissent-Funel, M.-C.; Hassanali, A.; Havenith, M.; Henchman, R.; Pohl, P.; Sterpone, F.; van der Spoel, D.; Xu, Y.; Garcia, A. E. Water Determines the Structure and Dynamics of Proteins. *Chem. Rev.* **2016**, *116*, 7673–7697.
- (21) Laage, D.; Elsaesser, T.; Hynes, J. T. Water Dynamics in the Hydration Shells of Biomolecules. *Chem. Rev.* **2017**, *117*, 10694–10725.
- (22) Aseyev, V.; Tenhu, H.; Winnik, F. M. *In Self Organized Nanostructures of Amphiphilic Block Copolymers II*; Springer: Berlin, Heidelberg, 2011; pp. 29–89.
- (23) Kojima, H. Studies on the phase transition of hydrogels and aqueous solutions of thermosensitive polymers. *Polym. J.* **2018**, *50*, 411–418.
- (24) Solhi, L.; Guccini, V.; Heise, K.; Solala, I.; Niinivaara, E.; Xu, W.; Mihhels, K.; Kröger, M.; Meng, Z.; Wohler, J.; Tao, H.; Cranston, E. D.; Kontturi, E. Understanding Nanocellulose-Water Interactions: Turning a Detriment into an Asset. *Chem. Rev.* **2023**, *123*, 1925–2015.
- (25) Etale, A.; Onyianta, A. J.; Turner, S. R.; Eichhorn, S. J. Cellulose: A Review of Water Interactions, Applications in Composites, and Water Treatment. *Chem. Rev.* **2023**, *123*, 2016–2048.
- (26) Hubbe, M. A.; Sjöstrand, B.; Lestelius, M.; Håkansson, H.; Swerin, A.; Henriksson, G. Swelling of cellulosic fibers in aqueous systems: A Review of chemical and mechanistic factors. *BioResources* **2024**, *19*, 6859–6945.
- (27) Sjöstrand, B.; Karlsson, C.-A.; Barbier, C.; Henriksson, G. Hornification in commercial chemical pulps: Dependence on drying temperature. *BioResources* **2024**, *19*, 7042–7056.
- (28) Laage, D.; Stirnemann, G.; Sterpone, F.; Rey, R.; Hynes, J. T. Reorientation and Allied Dynamics in Water and Aqueous Solutions. *Annu. Rev. Phys. Chem.* **2011**, *62*, 395–416.
- (29) Philipp, M.; Kyriakos, K.; Silvi, L.; Lohstroh, W.; Petry, W.; Krüger, J. K.; Papadakis, C. M.; Müller-Buschbaum, P. From Molecular Dehydration to Excess Volumes of Phase-Separating PNIPAM Solutions. *J. Phys. Chem. B* **2014**, *118*, 4253–4260.
- (30) O’Neill, H.; Pingali, S. V.; Petridis, L.; He, J.; Mamontov, E.; Hong, L.; Urban, V.; Evans, B.; Langan, P.; Smith, J. C.; et al. Dynamics of water bound to crystalline cellulose. *Sci. Rep.* **2017**, *7*, 11840.
- (31) Tan, P.; Liang, Y.; Xu, Q.; Mamontov, E.; Li, J.; Xing, X.; Hong, L. Gradual Crossover from Subdiffusion to Normal Diffusion: A Many-Body Effect in Protein Surface Water. *Phys. Rev. Lett.* **2018**, *120*, 248101.
- (32) Guccini, V.; Yu, S.; Meng, Z.; Kontturi, E.; Demmel, F.; Salazar-Alvarez, G. The Impact of Surface Charges of Carboxylated Cellulose Nanofibrils on the Water Motions in Hydrated Films. *Biomacromolecules* **2022**, *23*, 3104–3115.
- (33) Tang, C.; Syafiqah, M.; Koh, Q.; Chun-Yi Ang, M.; Choo, K.; Sun, M.; Callsen, M.; Feng, Y.; Chua, L.; Png, R.; et al. Water binding and hygroscopicity in π -conjugated polyelectrolytes. *Nat. Commun.* **2023**, *14*, 3978.
- (34) Kreuzer, L. P.; Widmann, T.; Bießmann, L.; Hohn, N.; Pantle, J.; Märkl, R.; Moulin, J.-F.; Hildebrand, V.; Laschewsky, A.; Papadakis, C. M.; Müller-Buschbaum, P. Phase Transition Kinetics of Doubly Thermoresponsive Poly(sulfobetaine)-Based Diblock Copolymer Thin Films. *Macromolecules* **2020**, *53*, 2841–2855.
- (35) Kreuzer, L. P.; Lindenmeir, C.; Geiger, C.; Widmann, T.; Hildebrand, V.; Laschewsky, A.; Papadakis, C. M.; Müller-Buschbaum, P. Poly(sulfobetaine) versus Poly(N-isopropylmethacrylamide): Co-Nonsolvency-Type Behavior of Thin Films in a Water/Methanol Atmosphere. *Macromolecules* **2021**, *54*, 1548–1556.
- (36) Niebuur, B.-J.; Lohstroh, W.; Appavou, M.-S.; Schulte, A.; Papadakis, C. M. Water Dynamics in a Concentrated Poly(N-isopropylacrylamide) Solution at Variable Pressure. *Macromolecules* **2019**, *52*, 1942–1954.
- (37) Betker, M.; Erichlandwehr, T.; Sochor, B.; Erbes, E.; Kurmanbay, A.; Alon, Y.; Li, Y.; Fernandez-Cuesta, I.; Müller-Buschbaum, P.; Teichert, S. A.; et al. Micrometer-Thin Nanocellulose Foils for 3D Organic Electronics. *Adv. Funct. Mater.* **2024**, *24*, 2403952.
- (38) Ono, Y.; Shikata, T. Contrary Hydration Behavior of N-Isopropylacrylamide to its Polymer, P(NIPAm), with a Lower Critical Solution Temperature. *J. Phys. Chem. B* **2007**, *111*, 1511–1513.
- (39) Rubio Retama, J.; Frick, B.; Seydel, T.; Stamm, M.; Fernandez Barbero, A.; López Cabarcos, E. Polymer Chain Dynamics of Core-

Shell Thermosensitive Microgels. *Macromolecules* **2008**, *41*, 4739–4745.

(40) Settles, M.; Doster, W. Anomalous diffusion of adsorbed water: a neutron scattering study of hydrated myoglobin. *Faraday Discuss* **1996**, *103*, 269–279.

(41) Malo de Molina, P.; Alvarez, F.; Frick, B.; Wildes, A.; Arbe, A.; Colmenero, J. Investigation of the dynamics of aqueous proline solutions using neutron scattering and molecular dynamics simulations. *Phys. Chem. Chem. Phys.* **2017**, *19*, 27739–27754.

(42) Bizzarri, A. R.; Cannistraro, S. Molecular Dynamics of Water at the Protein-Solvent Interface. *J. Phys. Chem. B* **2002**, *106*, 6617–6633.

(43) Sokolov, A.; Grimm, H.; Kisliuk, A.; Dianoux, A. Slow Relaxation Process in DNA. *J. Biol. Phys.* **2001**, *27*, 313–327.

(44) Doster, W.; Gebhardt, R. High pressure - unfolding of myoglobin studied by dynamic neutron scattering. *Chem. Phys.* **2003**, *292*, 383–387. Quasielastic Neutron Scattering of Structural Dynamics in Condensed Matter.

(45) Buchner, R.; Barthel, J.; Stauber, J. The dielectric relaxation of water between 0°C and 35°C. *Chem. Phys. Lett.* **1999**, *306*, 57–63.

(46) Zaslavsky, A. Y. Dielectric Relaxation in Liquid Water: Two Fractions or Two Dynamics? *Phys. Rev. Lett.* **2011**, *107*, 117601.

(47) Vinh, N. Q.; Doan, L. C.; Hoang, N. L. H.; Cui, J. R.; Sindle, B. Correlation between macroscopic and microscopic relaxation dynamics of water: Evidence for two liquid forms. *J. Chem. Phys.* **2023**, *158*, 204507.

(48) Popov, I.; Ishai, P. B.; Khamzin, A.; Feldman, Y. The mechanism of the dielectric relaxation in water. *Phys. Chem. Chem. Phys.* **2016**, *18*, 13941–13953.

(49) Ohmine, I. Liquid Water Dynamics: Collective Motions, Fluctuation, and Relaxation. *J. Phys. Chem.* **1995**, *99*, 6767–6776.

(50) Walrafen, G. E.; Chu, Y. C. Linearity between Structural Correlation Length and Correlated-Proton Raman Intensity from Amorphous Ice and Supercooled Water up to Dense Supercritical Steam. *J. Phys. Chem.* **1995**, *99*, 11225–11229.

(51) Wan, Q.; Spanu, L.; Galli, G. A.; Gygi, F. Raman Spectra of Liquid Water from Ab Initio Molecular Dynamics: Vibrational Signatures of Charge Fluctuations in the Hydrogen Bond Network. *J. Chem. Theory Comput.* **2013**, *9*, 4124–4130.

(52) Wang, J. H. Self-Diffusion Coefficients of Water. *J. Phys. Chem.* **1965**, *69*, 4412–4412.

(53) Yoshida, K.; Matubayasi, N.; Nakahara, M. Self-diffusion coefficients for water and organic solvents at high temperatures along the coexistence curve. *J. Chem. Phys.* **2008**, *129*, 214501.

(54) Kikuchi, T.; Nakajima, K.; Ohira-Kawamura, S.; Inamura, Y.; Yamamuro, O.; Kofu, M.; Kawakita, Y.; Suzuya, K.; Nakamura, M.; Arai, M. Mode-distribution analysis of quasielastic neutron scattering and application to liquid water. *Phys. Rev. E* **2013**, *87*, 062314.

(55) Singwi, K. S.; Sjölander, A. Diffusive Motions in Water and Cold Neutron Scattering. *Phys. Rev.* **1960**, *119*, 863–871.

(56) Ghugare, S. V.; Chiessi, E.; Telling, M. T. F.; Deriu, A.; Gerelli, Y.; Wuttke, J.; Paradossi, G. Structure and Dynamics of a Thermoresponsive Microgel around Its Volume Phase Transition Temperature. *J. Phys. Chem. B* **2010**, *114*, 10285–10293.

(57) Qvist, J.; Schober, H.; Halle, B. Structural dynamics of supercooled water from quasielastic neutron scattering and molecular simulations. *J. Chem. Phys.* **2011**, *134*, 144508.

(58) Teixeira, J.; Bellissent-Funel, M.-C.; Chen, S. H.; Dianoux, A. J. Experimental determination of the nature of diffusive motions of water molecules at low temperatures. *Phys. Rev. A* **1985**, *31*, 1913–1917.

(59) Bove, L. E.; Klotz, S.; Strässle, T.; Koza, M.; Teixeira, J.; Saitta, A. M. Translational and Rotational Diffusion in Water in the Gigapascal Range. *Phys. Rev. Lett.* **2013**, *111*, 185901.

(60) Brett, C. J.; Mittal, N.; Ohm, W.; Gensch, M.; Kreuzer, L. P.; Körstgens, V.; Månsson, M.; Frielinghaus, H.; Müller-Buschbaum, P.; Söderberg, L. D.; Roth, S. V. Water-Induced Structural Rearrangements on the Nanoscale in Ultrathin Nanocellulose Films. *Macromolecules* **2019**, *52*, 4721–4728.

(61) Belaine, D.; Andreasen, J. W.; Palisaitis, J.; Malti, A.; Håkansson, K.; Wågberg, L.; Crispin, X.; Engquist, I.; Berggren, M. Controlling the Organization of PEDOT: PSS on Cellulose Structures. *ACS Appl. Polym. Mater.* **2019**, *1*, 2342–2351.

(62) Chan, E. P.; Frieberg, B. R.; Ito, K.; Tarver, J.; Tyagi, M.; Zhang, W.; Coughlin, E. B.; Stafford, C. M.; Roy, A.; Rosenberg, S.; Soles, C. L. Insights into the Water Transport Mechanism in Polymeric Membranes from Neutron Scattering. *Macromolecules* **2020**, *53*, 1443–1450.

(63) Nečas, D.; Klapetek, P. Gwyddion: an open-source software for SPM data analysis. *Cent. Eur. J. Phys.* **2012**, *10*, 181–188.

(64) Kreuzer, L. P.; Betker, M.; Ollivier, J.; Roth, S. V.; Söderberg, L. D.; Wolf, M. QENS study on the water and polymer side chain dynamics in PEDOT: PSS/cellulose nanofibril films; Institut Laue-Langevin. DOI: .

(65) Ollivier, J.; Mutka, H. INS Cold Neutron Time-of-Flight Spectrometer, Prepared to Tackle Single Crystal Spectroscopy. *J. Phys. Soc. Jpn.* **2011**, *80*, SB003.

(66) Arnold, O.; et al. Mantid-Data analysis and visualization package for neutron scattering and μ SR experiments. *Nucl. Instrum. Methods Phys. Res., Sect. A* **2014**, *764*, 156–166.

NOTE ADDED AFTER ASAP PUBLICATION

This paper was published ASAP on February 18, 2025. Figure 3 was replaced and the corrected version was reposted on February 19, 2025.